PROCEEDINGS, 50th Workshop on Geothermal Reservoir Engineering
Stanford University, Stanford, California, February 10-12, 2025
SGP-TR-229

Updated Modelling of the Salton Sea Geothermal Field

Theo Renaud, Adrian Croucher, Ken Dekkers, Michael Gravatt, Michael O'Sullivan, Joris Popineau, Jeremy Riffault, Ryan Tonkin and John O'Sullivan

Department of Engineering Science, University of Auckland, 70 Symonds Street, Grafton, Auckland, 1010, New Zealand

theo.renaud@auckland.ac.nz

Keywords: Reservoir modeling, geothermal simulator, Waiwera, uncertainty quantification, lithium, Salton Sea

ABSTRACT

The Salton Sea Geothermal Field (SSGF) is one of the world's largest geothermal resources with an estimated resource potential of nearly 3 GW and dissolved minerals such as lithium of high interest. Despite a long history of production from and reinjection into the deep geothermal system, the brine's complex high salinity is challenging in assessing future operations and planning the management of the SSGF.

New developments on the SSGF are ongoing to exploit the deep geothermal system for geothermal energy production and to use the lithium-rich geothermal brine as a source of lithium for battery production.

We present an updated numerical model of the SSGF field using a chloride-NCG-water equation of state with lithium as a passive tracer. Based on our previous modelling approach representing the production history and future scenarios (Araya and O Sullivan, 2022, Dobson et al., 2023, O Sullivan et al., 2023a) we have refined the model grid to provide a more accurate match of the reinjection returns and chemical breakthrough by reinjection fluid with a diluted lithium content. Publicly available data were used to calibrate the updated model for both the natural state and production history. A preliminary uncertainty quantification of the updated model has been carried out varying the key unknown parameters (porosities, permeabilities, upflows). The results provide an improved understanding of the SSGF and demonstrate the capability of uncertainty quantification for providing robust ranges of forecasts, including rates of lithium extraction.

The results highlight the need for robust, integrated geothermal reservoir modelling with uncertainty quantification to support planning the sustainable utilization of geothermal energy and extraction of lithium from the SSGF.

1. INTRODUCTION

The Salton Sea area is located in southern California, as shown in Figure 1. This unique environment is an active pull-apart basin straddling the North American and Pacific Plates. The Salton Trough is a continental rift zone where a series of right-stepping dextral faults link the East Pacific Rise to the San Andreas fault system, leading to the existence of spreading centers in the extensional gaps (Dorsey, 2006, Hulen et al., 2002).

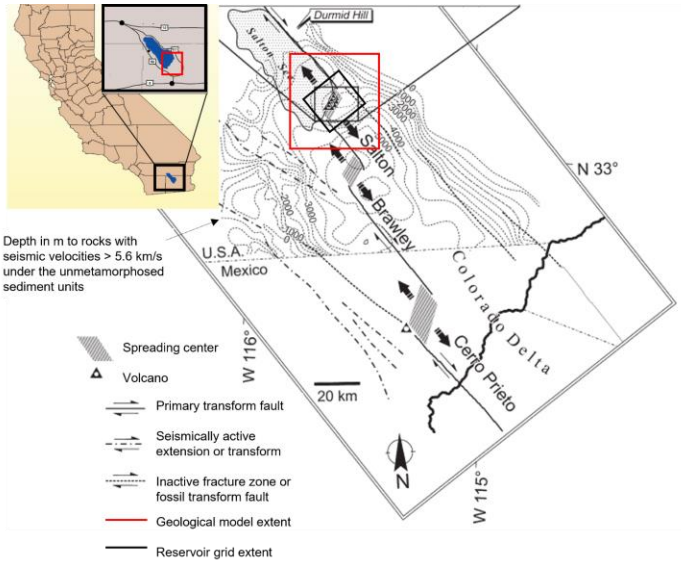

Figure 1: Location of the Salton Sea area, the geological model and the extent of the reservoir model grid (Map modified from Schmitt and Hulen 2008).

The area has a background heat flux of greater than 100 mW/m^2 (Lachenbruch et al., 1985) with higher heat flows of greater than 500 mW/m^2 in zones concentrated in the SSGF. The high heat flows are due to local Quaternary volcanism associated with upwelling of hydrothermal fluids (Sass et al., 1984) associated with deep magmatic intrusions induced by the crustal thinning. Metamorphism and hydrothermal alteration processes resulting from the hot fluid circulation in the area occur at shallower depths in the SSGF (~1.5 km) within the thick Colorado River sediment pile (Han et al., 2016).

The high concentration of salt and other dissolved solids are one of the key characteristics of the deep reservoir of the SSGF. Two approximate layers of salinity distribution are observed with a cooler less saline brine (< 10 wt.% TDS) overlaying a hot hypersaline brine (> 20 wt.% TDS). An active convection and a relatively long residence time are estimated for the SSGF due to the brine isotopic and chemical compositions (Williams and McKibben, 1989). Dissolved metals, notably Li are highly concentrated in the hypersaline brines (> 200 ppm). The energy demand for renewable electricity and the potential to extract dissolved lithium provide unique opportunities for the SSGF. These opportunities have triggered fundamental research to quantify the complex behavior of the SSGF including the use of accurate numerical modeling.

Preliminary modeling results have been presented previously (Araya and O'Sullivan, 2022, Dobson et al., 2023, O'Sullivan et al. 2023a, O'Sullivan et al. 2024). This work presents an updated numerical model and modeling results including:

- Increased model resolution in the production zone
- Revised conceptual understanding of the area with data collection and improve definitions of the alteration zones
- Improved model calibration
- Uncertainty quantification of model forecasts

2. CONCEPTUAL MODEL

2.1 Geological context

Figure 2 shows the seven geologic units considered in the model. Chronologically, from the youngest to the oldest, the following formations have been defined based on previous research (see Araya and O'Sullivan, 2022 and references therein): Alluvium, Brawley Formation, Upper and Lower Borrego, Palm Springs Formation, Imperial Group, Crystalline Basement. The thicknesses of the units were interpreted from regional stratigraphic cross-sections and seismic velocity transitions occurring at ~1.5 km depths beneath the center of the SSGF. The Salton Sea sub-basin is hosting a complex structural fault network, as shown in the numerical model in Araya and O'Sullivan (2022).

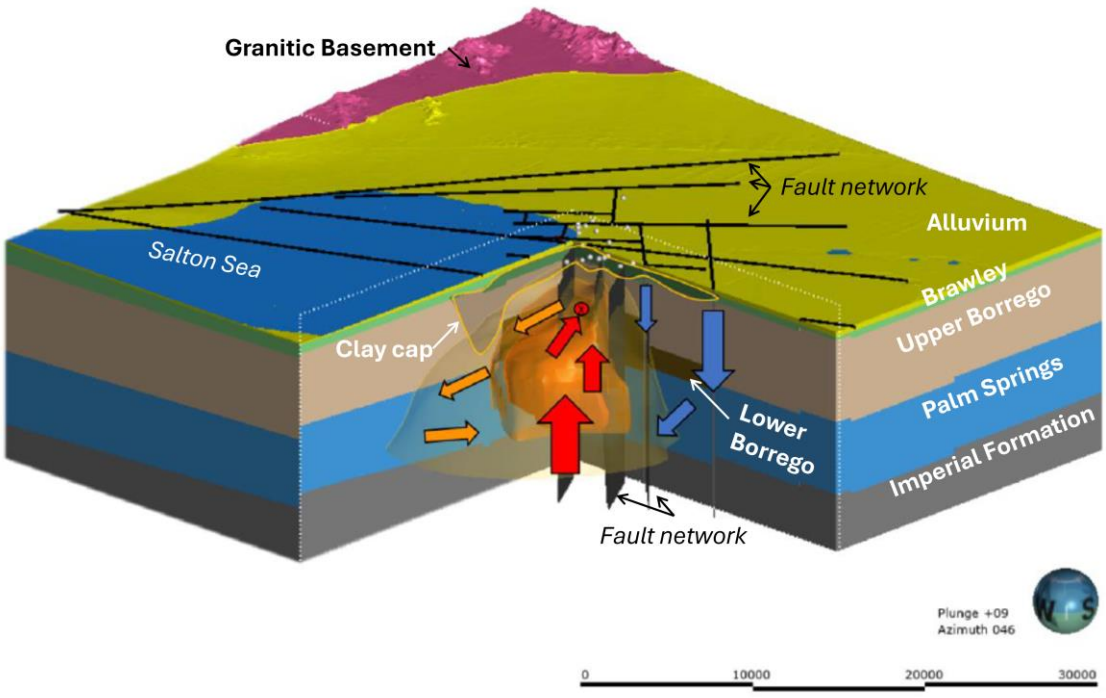

Figure 2: Conceptual model of the Salton Sea Geothermal Field (modified from Araya and O'Sullivan, 2022). The rocks formations are shown in white along with the fault network, the clay cap and the Salton Sea area. Red arrows show hot upflow and blue arrows show cold down flow.

2.2 Alteration model

Four 2D land and offshore resistivity profiles from Nichols (2009) were used to digitally construct the clay cap in the conceptual model. Figure 3 shows the alteration zones defined as the extremely conductive zone (0.2 to 0.4 Ohm-m). Some uncertainty in the location of the clay cap exists as a combination of high temperature, high salinity, and high porosity can also produce very low resistivity values (Nichols, 2009). Further analysis and refinements are being considered based on more recent acquisitions.

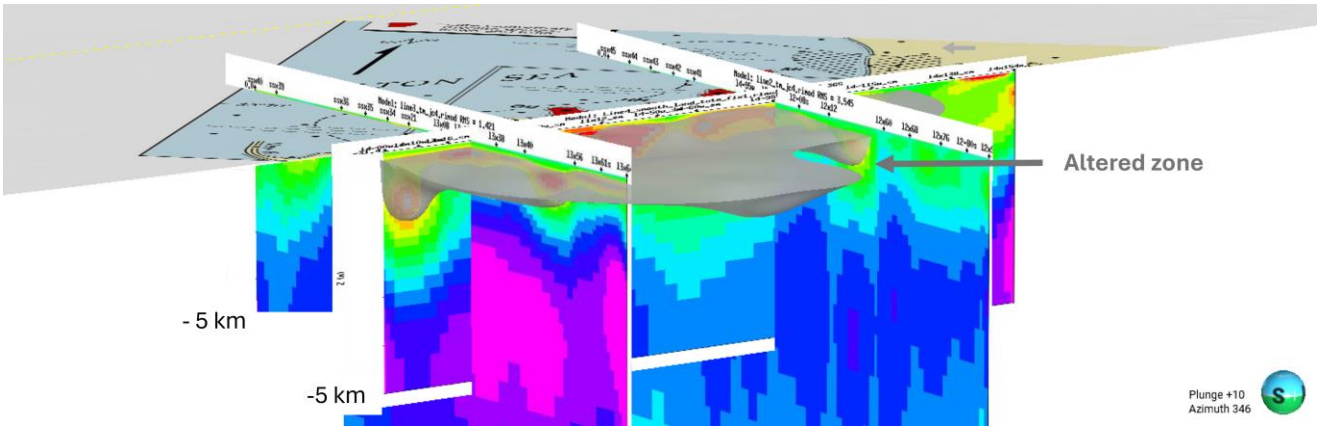

Figure 3: Interpreted Altered zone (Clay cap) in the numerical model and MT profiles from Nichols (2009).

2.3 Chemical distribution

Based on the work of Williams and McKibben (1989) and the collection of chemical data from the Department of Conservation of California, (CalGEM's GeoSteam database, 2022), the conceptual understanding of the temperature and chemical distribution can be distributed into three zones:

- The Distal zone, located at the outer boundary of the SSGF, with conductive regimes and low salinity gradient until 2 km depth.
- The Central region with a high convective temperature profile, with up to 300-320°C at 500-700 meter depth and >20 wt.% TDS.
- The Boundary region shows slightly lower downhole temperature profiles compared to the central region with an intermediate chemical composition with a transition zone below 1 km depth.

This chemical distribution is helpful for evaluating the accuracy of the model's representation of the thermodynamic behavior of the fluids in the SSGS and its lithium content in the high salinity brines.

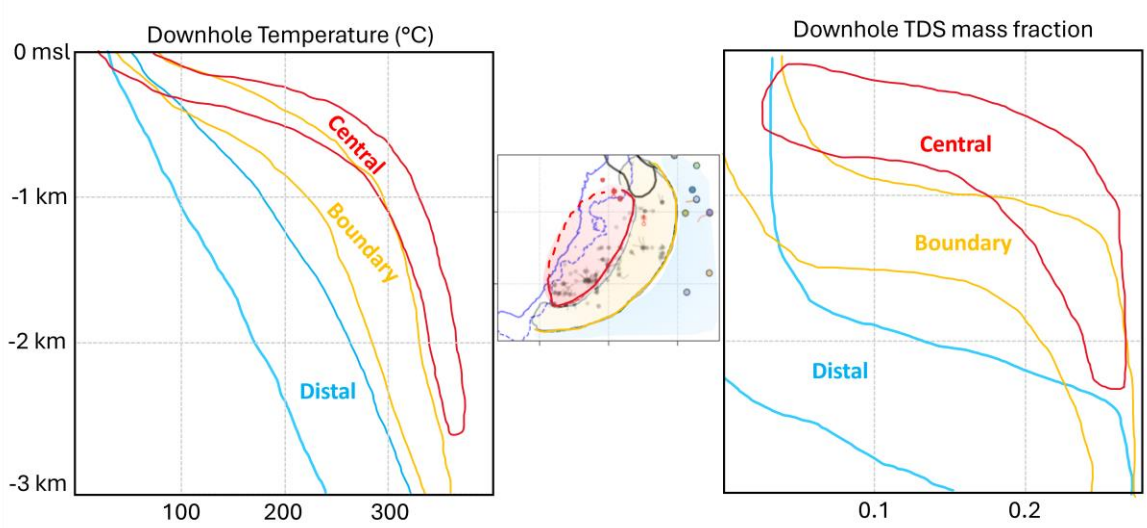

Figure 4: Downhole temperature and total dissolved fluids (salinity gradients) in the Central area, the Boundary area and the Distal area of the SSGF (modified from Williams and McKibben 1989). (Center) Map of the SSGF with the Central, Boundary and Distal area colored respectively in red, orange and blue. Well locations are shown in grey.

3. NUMERICAL MODEL DESIGN

The 3D conceptual model was discretized into a block model for applying mass and energy balance calculations using the Waiwera geothermal simulator (Croucher et al., 2020). The model was run in the Cloud using 96 core high-performance compute nodes on Amazon Web Services (AWS) (O'Sullivan et al. 2024). Figure 5 shows a plan view of the grid which has the same extent and orientation as the previous model with dimensions of 24 x 24 x 3 km. It is oriented to align with the NE trending axis of the Main Central Fault Zone (Araya and O'Sullivan 2022).

The updated grid has two levels of refinement: 200 x 200m in the central area of the SSGF, 400 x 400m on its near periphery and 800 x 800m in the remainder of the model. Twenty-nine layers are used in the model with a vertical refinement of 15 m near the surface, 50m at the water table, 10 m in the upper reservoir (-500 to -1500 msl), 200m in the lower reservoir (-1500 to -2500 msl), and 500m at the greatest depths below -2500 msl. At the surface the grid follows the topography resulting in a total of 93,186 blocks.

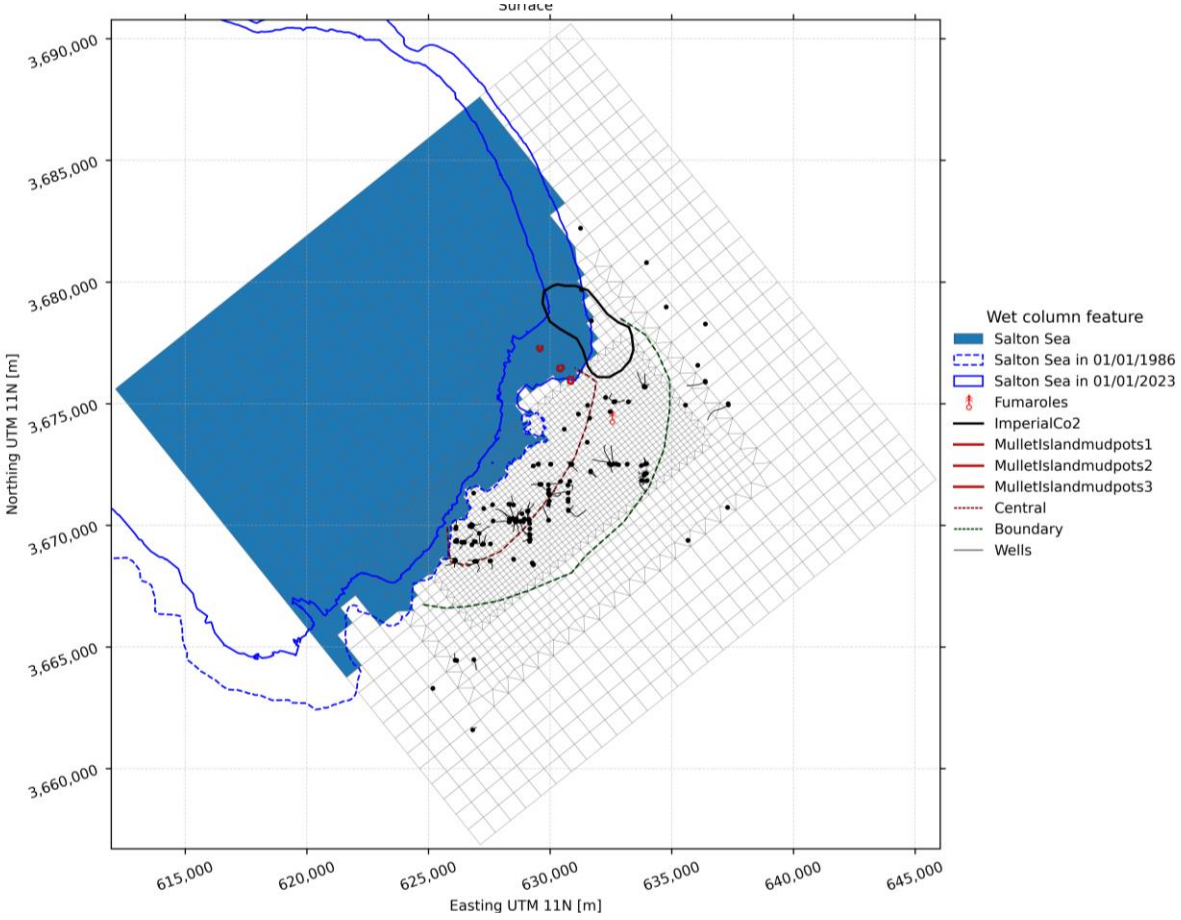

Figure 5: Plan view of the updated model grid showing the well tracks and wet columns (i.e. Salton Sea). Central and Boundary zones show the limits of the thermal dome indicated by Williams (1997). Fumaroles and the Mullet Island mudpots are referenced Lynch and Hudnut (2008). The Imperial CO_2 contour, a zone with higher surface CO_2 concentration, is taken from Muffler and White (1968).

The EWASG equation of state in Waiwera was used to include salinity and CO_2 in the thermodynamic calculations and lithium was included in the model as a passive tracer. The top of the model was assigned dry atmospheric conditions of 1 bar and a mean temperature of 23°C on land and a wet atmosphere for the Salton Sea with a temperature of 23°C and a pressure determined by the depth of the sea. The chloride concentration of the Salton Sea was set to a mass fraction of 50,000 ppm.

At the base of the model a background heat flux of 150 mW/m^2 was applied, with 230 and 310 mW/m^2 in the periphery and central part of the SSGF respectively. Chloride was included in the deep upflows at a mass fraction equivalent to 152,000 ppm and lithium at a concentration of 220 ppm, a ratio of 682:1. The side boundaries of the grid are set as a hydrostatic temperature gradient with a low salt and CO_2 mass fraction at depth approximating the deep Salton Trough conditions.

The updated model uses 558 rock-types covering the combinations of lithologies, faults, fault intersections, and an alteration zone that are included in the conceptual model. Many rock-type classifications share common permeability and porosity values, but the large number of combinations allows a high level of heterogeneity in the permeability and porosity distributions (O'Sullivan et al. 2023b). Other secondary rock properties (density, thermal conductivity, and rock grain-specific) were assumed to be uniform across all rock-type classifications. For production, a dual-porosity model was used to capture reinjection returns more accurately. The dual-porosity parameters are given in Table 1 below.

Table 1: Dual porosity parameters used in the production history model

Parameters	Value
Number of matrix blocks	2 (20% and 77.5% volume fraction)
Volume fraction of fracture blocks	2.5%
Fracture spacing - number of planes	25m spacing with 3 planes
Permeability of matrix	1.0E-16 m^2
Permeability of fractures	variable
Porosity of fractures	80 %

4. UPDATED CALIBRATION DATA FOR THE SSGF

The previous model considered data from 90 wells with 28 production wells and 42 reinjection wells for calibration (Araya and O'Sullivan, 2022). Figure 6 presents the updated total production and injection mass flow dataset compared to the previous dataset used and the model results from O'Sullivan et al. (2024). The revised dataset is a result of a more detailed analysis of monthly reports from the CalGEM GeoSteam (2022) database, notably for the 1990s, where early production and reinjection data was missing in the previous dataset.

In the updated dataset, we consider historical data for 153 wells, including 62 production wells and 57 reinjection wells, (5 both reinjected and produced in the past). Measured CO_2 and lithium concentrations from the literature were also added to the calibration dataset for the updated numerical model.

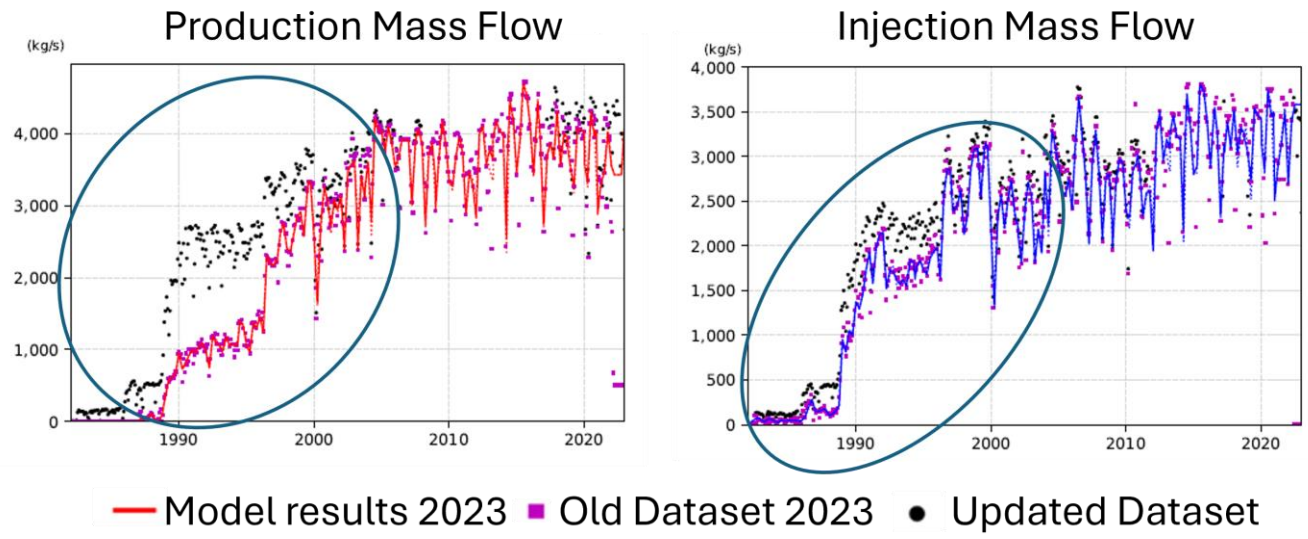

Figure 6: Total production (left) and injection (right) datasets compared with previous model results.

5. NATURAL STATE MODEL RESULTS

The current results of the natural state for the updated model are shown in Figure 7. Calibration is ongoing but so far, the early downhole temperature measurements in the Central and Boundary areas are well matched in some parts of the model, but need to be improved near the Magma Max cluster and further towards the boundary of the system as shown by the well Britz 3.

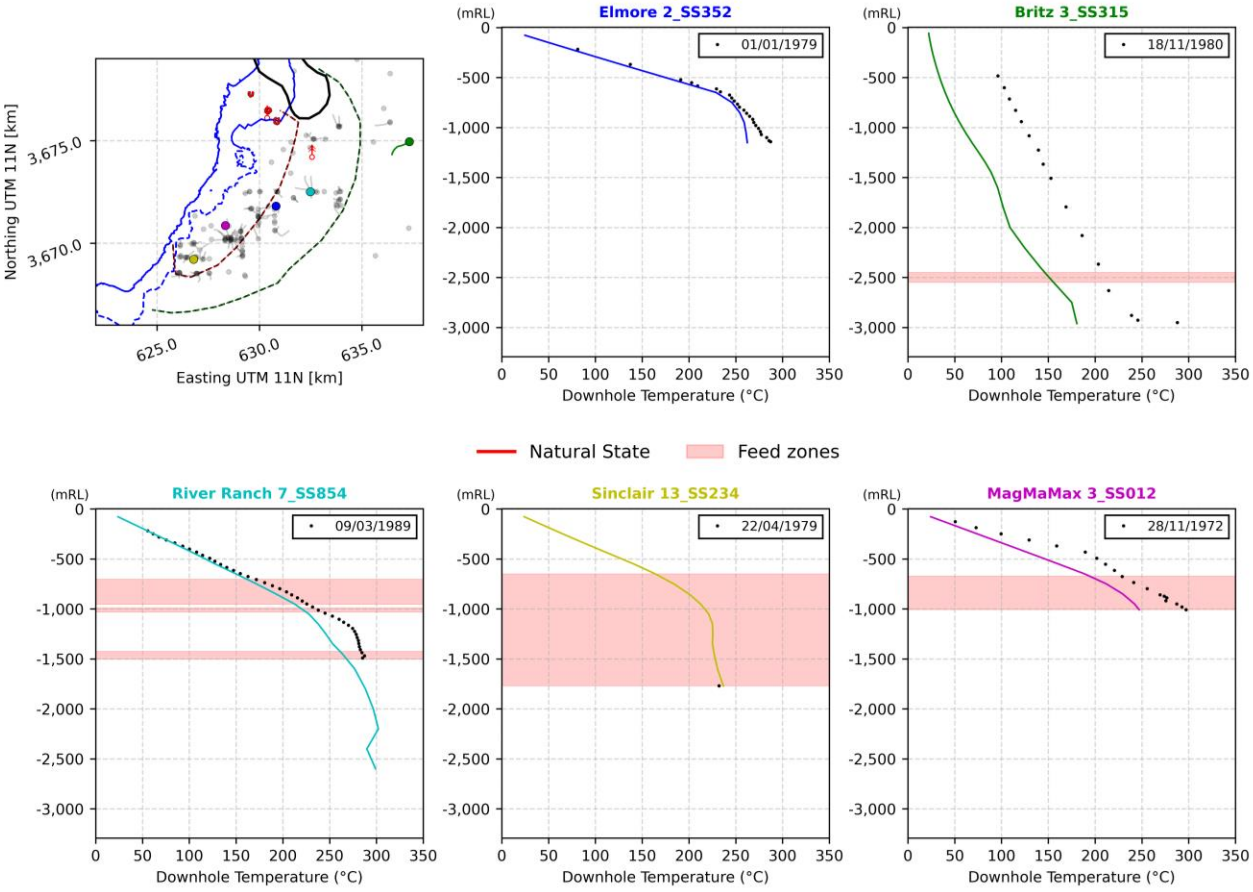

Figure 7: Natural State downhole temperature results for five representative wells in the SSGF.

Figure 8 presents the comparison of the downhole natural state Total Dissolved Solids (TDS) in the updated model with the estimated distributions in the regions defined by Williams and McKibben (1997). The TDS has been calculated using the chloride mass fraction in the reservoir model as a proxy (chloride content = 60 % of the TDS).

Despite the need for more calibration to improve the match to the data, the results achieved are already satisfying with respect to the conceptual understanding of the area discussed in Figure 4. The higher salt concentration at depth extending to the shallow elevations in the central regions has been captured. Similarly, the decrease in salt concentration towards the East (Boundary and Distal Region), has been achieved, with further local calibration required. The resulting calibrated permeability structure has a high ratio of horizontal to vertical permeabilities, varying from 1:10 to 1:100, with higher permeability vertical conduits provided by structures identified in the conceptual model. The altered formations at shallow depth in the clay cap, with low permeabilities prevent the hot brines from reaching the surface.

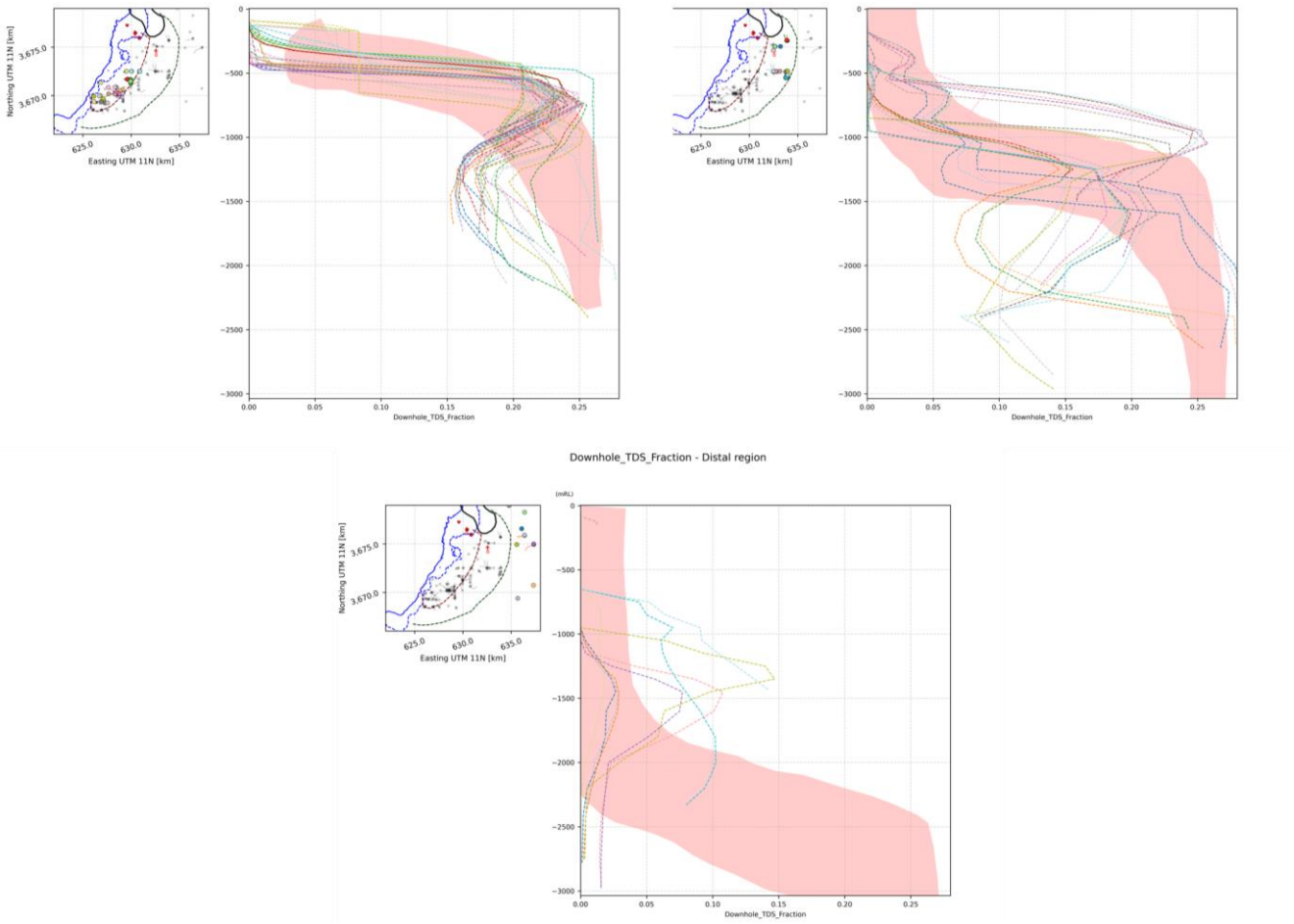

Figure 8: Natural state downhole total dissolved solid distribution for the updated numerical model of the SSGF compared with the Central, Boundary and Distal regions as described by Williams and McKibben (1997). Well locations given in the maps are colored corresponding to model results.

6. PRODUCTION HISTORY RESULTS

Figure 9 shows some production history results from the updated model for a representative well IID 16. The figure is taken from our standardized report which plots model results for each production well individually to check comparisons of the total salt mass fraction, lithium concentration, CO_2 mass fraction and total fluid enthalpy with available measured production data.

As this example shows, the quality of the match between model results and historical data is already good for many wells. However, local calibration improvements are required for other production wells and calibration is ongoing.

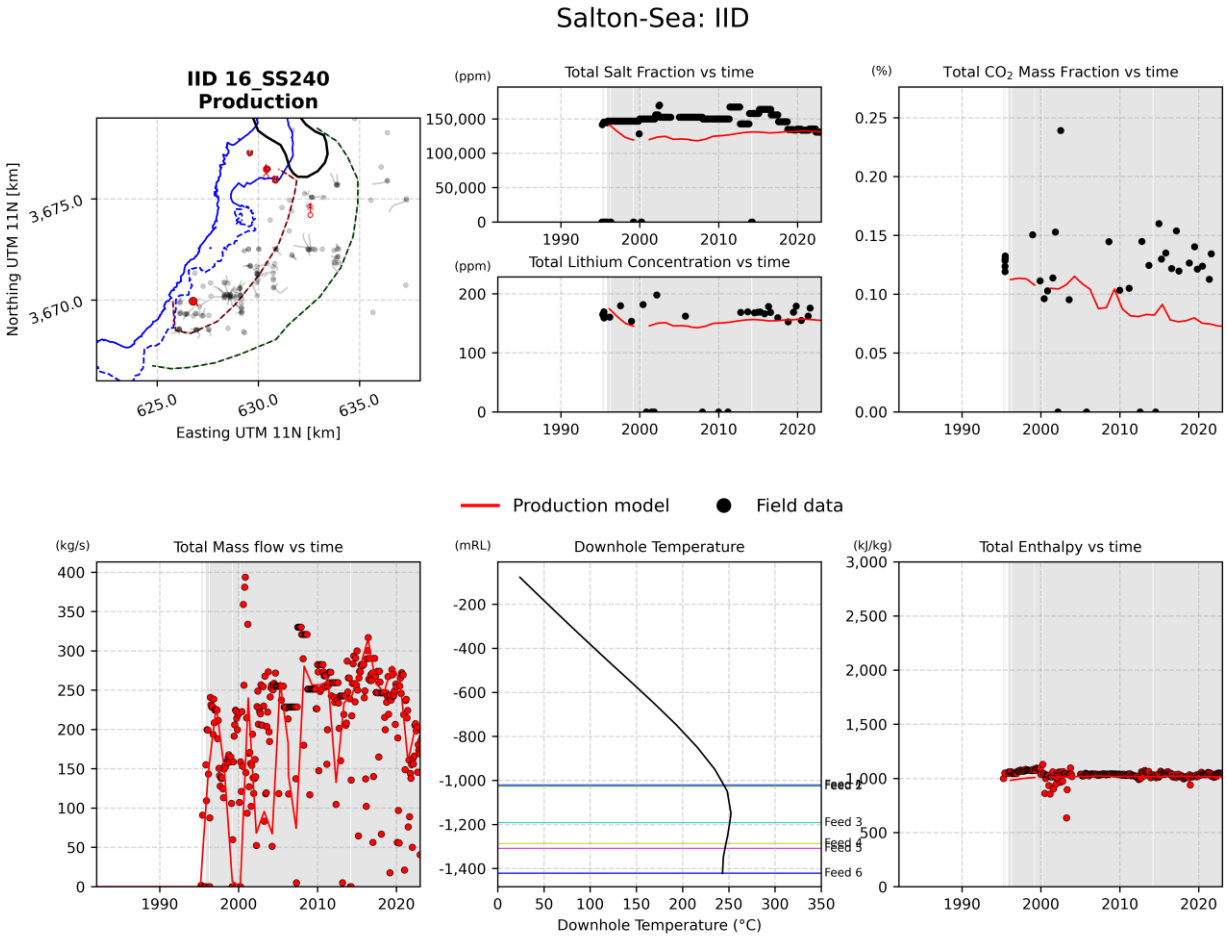

Figure 9: Production history model results for an example well IID 16.

7. UNCERTAINTY QUANTIFICATION SETUP

The simulations were carried out using Waiwera our highly parallelized and efficient geothermal simulator, on high-performance computers cloud based architecture provided by AWS. The ability to run hundreds of sample model quickly, cheaply and reliably provides an important new tool for investigating the behavior of the SSGF and understanding the observed data. In this work, we generated 200 sample models by varying the strength, location and chemical composition of the deep geothermal upflows and by varying permeability and porosity distributions.

By following our standard modelling framework (O'Sullivan et al. 2023b) and the uncertainty quantification approach described in Dekkers et al., (2022a), realistic distributions for the permeabilities and the porosities for each of the geological units, the altered formations and the intersection of the structural settings were generated for the SSGF. Similarly, realistic distributions of the potential strength, location and chemical composition of the deep geothermal upflows were generated.

Our resources assessment method then generated unconditioned sample models (prior distribution) by sampling from the distributions of the parameters. Examples of the distributions of permeabilities (k1,k2,k3 for the three spatial directions) and porosity probability for a selected model rock type are shown in Figure 10**Error! Reference source not found.**. Examples of the distributions of deep geothermal upflows from 3 sample models are shown in Figure 11.

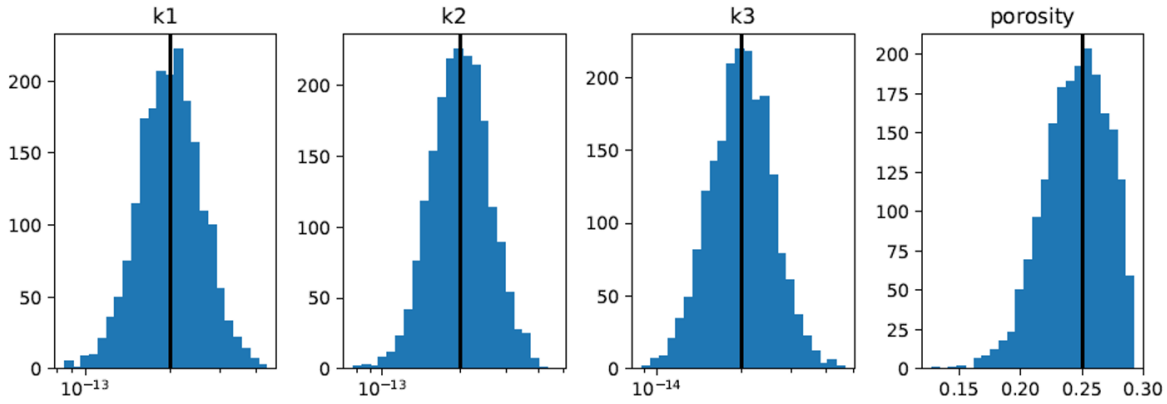

Figure 10: An example of the permeability and porosity distributions generated for one of the model rock types.

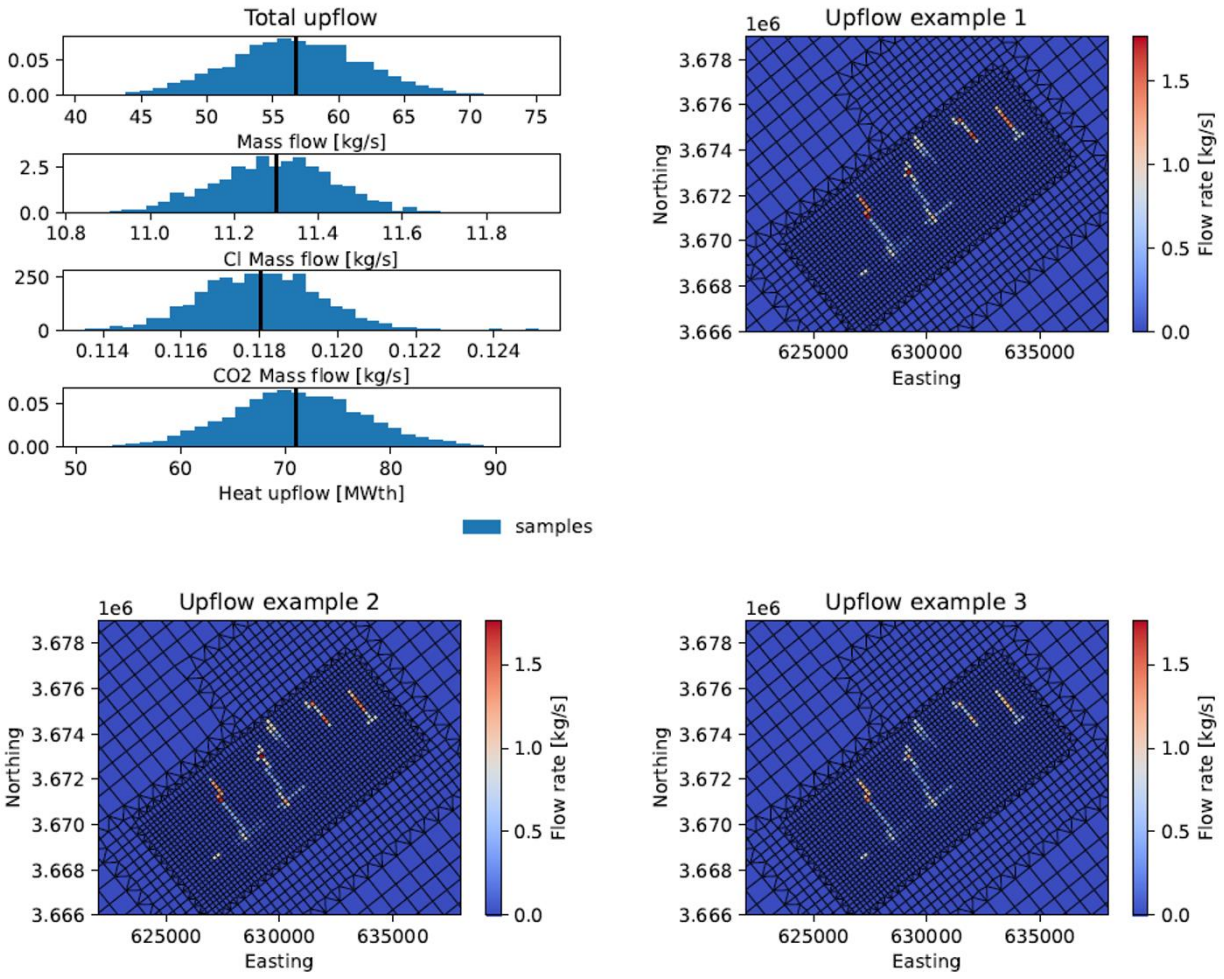

Figure 11: Water, chloride and CO_2 upflows distribution of the samples. Examples shown for 3 samples.

8. UNCERTAINTY QUANTIFICATION RESULTS

The objective of this preliminary uncertainty quantification was to test our established approach (Dekkers et al., 2022a, Dekkers et al., 2022b) when including chemical composition in the parameter distribution and the resulting forecast ranges. Therefore, a limited number of sample models were generated and a limited calibration dataset was used to select the models for forecasting.

A total of 200 sample models were set up by sampling from the parameter distributions and natural state simulations run for each of them. The 100 sample models that best agree with the natural state temperature data were then selected using the Approximate Bayesian Computation method described in Dekkers et al. (2022a) and Dekkers et al. (2022b). Note that in the future, all available calibration data will be used to select the models taken forward for forecasting.

The results of the preliminary uncertainty quantification analysis are shown in Figure 12 and Figure 13. They respectively show the distribution of forecast natural state downhole temperature distributions for selected wells and the distribution of forecast production history results for well IDD 16. The plots in Figure 13 show the power of our uncertainty quantification approach and its ability to produce accurate ranges of forecasts that can support decision-making and reservoir management.

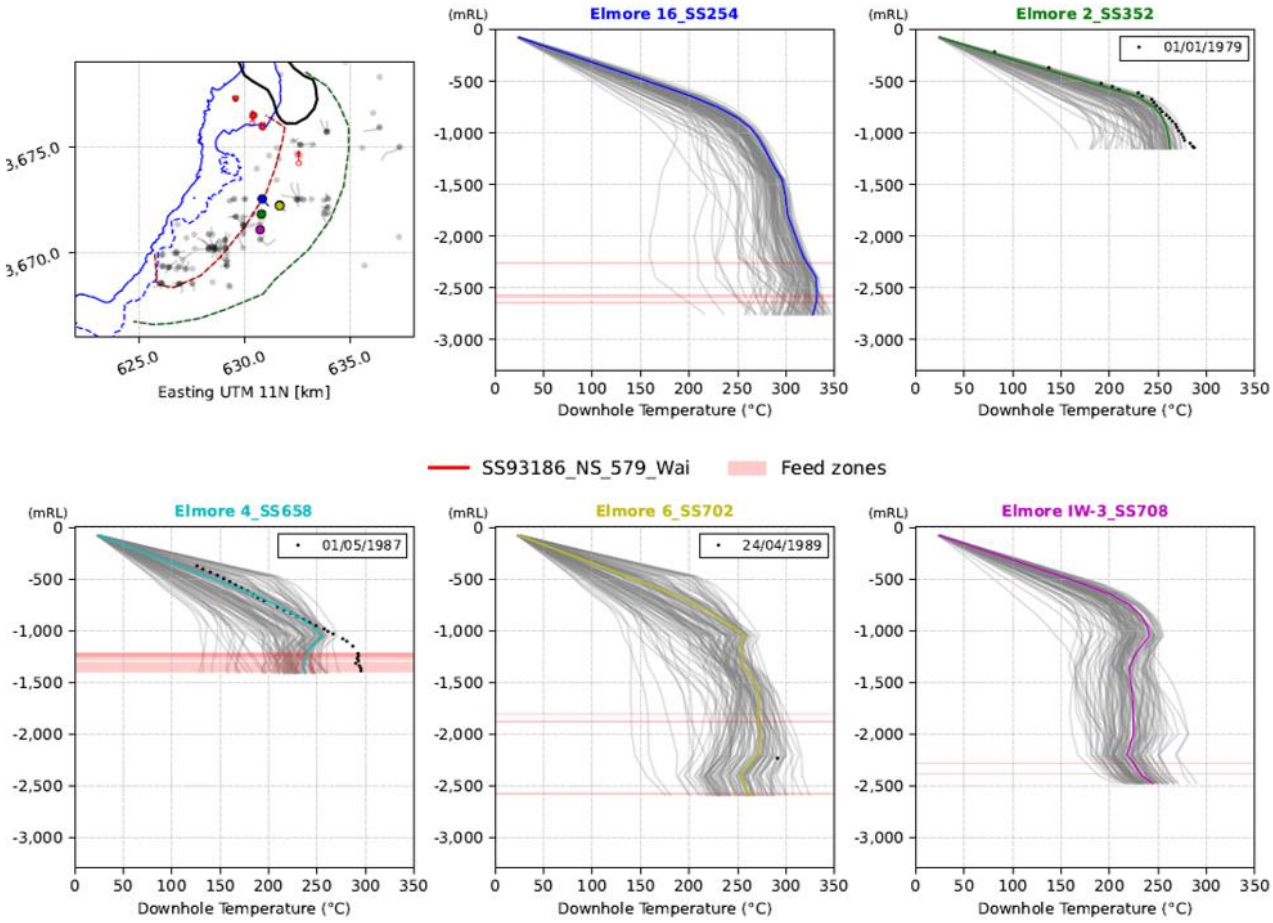

Figure 12: Forecast natural state downhole temperature distributions for selected wells using uncertainty quantification.

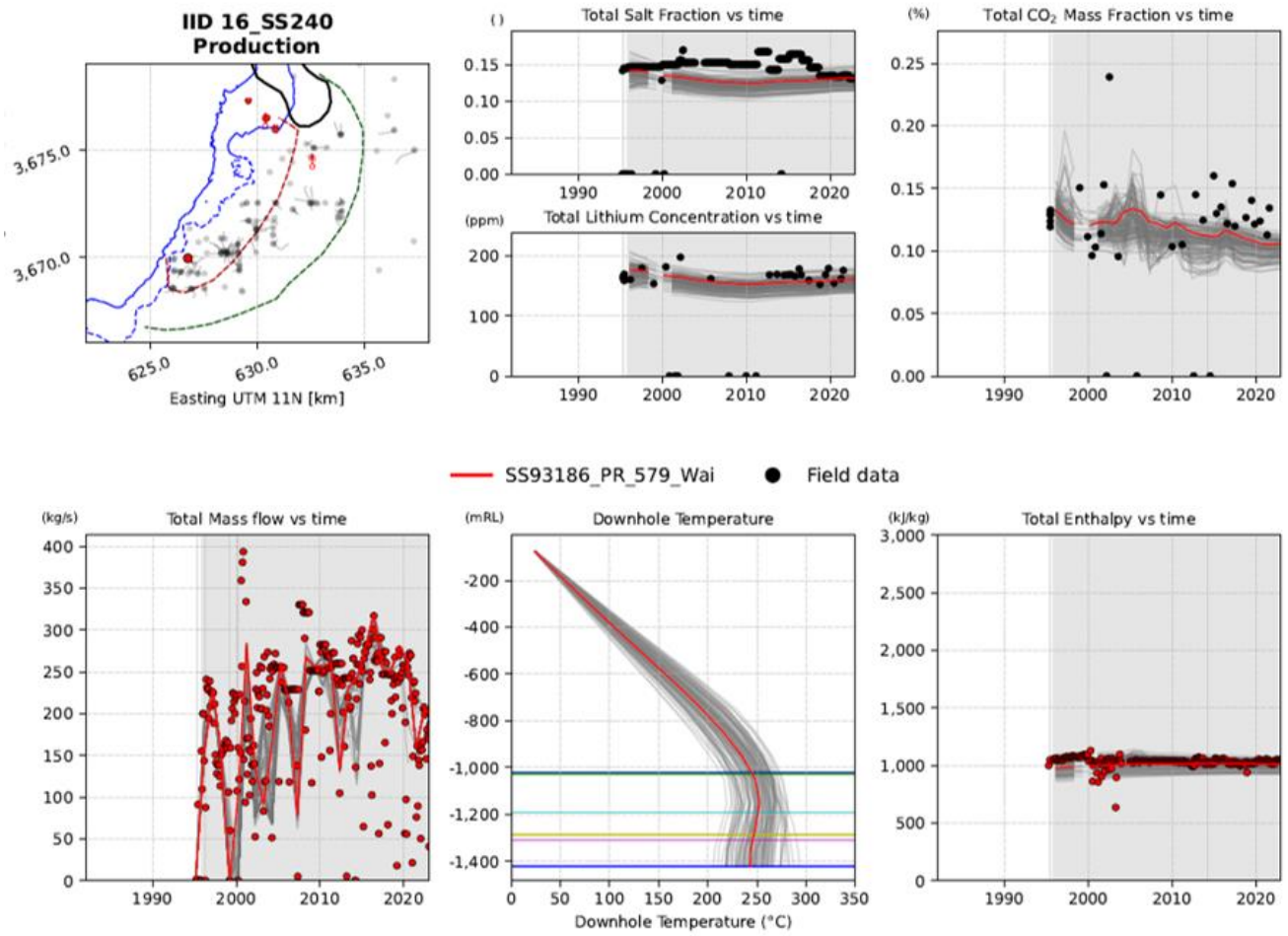

Figure 13: Distribution of production history forecasts provided by the uncertainty quantification for IID 16.

9. CONCLUSIONS

We have developed a detailed, integrated model of the SSGF to investigate the energy recovery and extraction of lithium-rich geothermal brine from the SSGF using an equation-of-state including water, chloride and CO_2. The usefulness of detailed modeling tools for supporting the management of the SSGF has been demonstrated (O'Sullivan et al., 2024). We are currently in a new phase of the project with the objective of updating the modeling tools to improve their accuracy, include uncertainty quantification and combine results with a technoeconomic analysis.

In this paper we have described the updated numerical model which includes a more refined grid in the central area of the SSGF, a larger, more complete calibration dataset, a revised the conceptual understanding of the area, improved model calibration, and a preliminary uncertainty quantification.

The results show that updated model provides a good representation of the SSGF though further calibration is required. The preliminary uncertainty quantification demonstrates the power of our uncertainty quantification approach and its ability to produce accurate ranges of forecasts that can support decision-making and reservoir management.

Following further model calibration and a full-scale uncertainty quantification will be carried out and the selected sample models will be used to generate ranges for forecasts for important possible future scenarios. The results from the forecasts will be used to support a technoeconomic analysis to support strategic decision-making for the sustainable management of the SSGF.

ACKNOWLEDGEMENTS

This work was supported by the U.S. Department of Energy, Office of Energy Efficiency and Renewable Energy (EERE), Office of Technology Development, Geothermal Technologies Office (GTO), under Award Number DE-AC02-05CH11231 with Lawrence Berkeley National Laboratory. The authors would also like to thank Seequent for their ongoing collaboration and support.

REFERENCES

Araya, N. and O'Sullivan, J. "A 3D Conceptual and Natural-State Model of the Salton Sea Geothermal Field." GRC Transactions, 46, (2022). 2123-2155.

CalGEM. "GeoSteam: Geothermal Well Records, Production and Injection Data [Data Files]." (2022). https://geosteam.conservation.ca.gov/

California Department of Conservation. "Geological Map of California [Data File]." (2015). https://maps.conservation.ca.gov/cgs/#datalist

California Department of Conservation. "Geothermal Production and Injection Data [Salton Sea]." (2022). https://www.conservation.ca.gov/calgem/geothermal/manual

Dekkers, K., Gravatt, M., Maclaren, O.J., Nicholson, R., Nugraha, R., O'Sullivan, M.J., Popineau, J., Riffault, J., O'Sullivan. J.P. Resource Assessment: Estimating the Potential of a Geothermal Reservoir. Proceedings: 47th Workshop on Geothermal Reservoir Engineering, Stanford University, Stanford, California, February 7-9, (2022a), SGP-TR-2231.

Dekkers, K., Gravatt, M., Renaud T., de Beer, A., Power, A., Maclaren, O.J., Nicholson, R., O'Sullivan, M., Riffault, J., O'Sullivan, J. Resource Assessment: Estimating the Potential of an African Rift Geothermal Reservoir. Proceedings, 9th African Rift Geothermal Conference, Djibouti, (2022b).

Dobson, P., Araya, N., Brounce, M., Busse, M., Camarillo, M. K., English, L., ... & White, M. (2023). Characterizing the Geothermal Lithium Resource at the Salton Sea. Lawrence Berkeley National Laboratory (LBNL), Berkeley, USA.

Dorsey, R. Stratigraphy, Tectonics, and Basin Evolution in the Anza-Borrego Desert Region. In G. T. Jefferson and L. Lindsay, Fossil Treasures of the Anza-Borrego Desert, Sunbelt Publication, (2006) 89-104.

Han, L., Hole, J.A., Stock, J.M., Fuis, G.S., Kell, A., Driscoll, N.W., Kent, G.M., Harding, A.J., Rymer, M.J., González-Fernández, A., and Lázaro-Mancilla, O.: Continental rupture and the creation of new crust in the Salton Trough rift, Southern California and northern Mexico: Results from the Salton Seismic Imaging Project. Journal of Geophysical Research: Solid Earth, 121, (2016), 7469-7489.

Hulen, J., Kaspereit, D., Norton, D.L., Osborn, W., Pulka, F.S. Refined Conceptual Modeling and a New Resource Estimate for the Salton Sea Geothermal Field, Imperial Valley, California. Geothermal Resources Council Transactions, 26, (2002), 29-36.

Lachenbruch, A.H., Sass, J.H., and Galanis, S.P. Jr.: Heat flow in southernmost California and the origin of the Salton Trough. Journal of Geophysical Research, 90 (B8), (1985), 6709-6736.

Lynch D.K., Hudnut, K.W.: The Wister Mud Pot Lineament: Southeastward Extension or Abandoned Strand of the San Andreas Fault ? Bulletin of the Seismological Society of America, 98 (2008), 1720-1729

Muffler, L.J.P., White, D.E.: Origin of CO2 in the Salton Sea geothermal system, southeastern California, USA. Proceedings 23rd Intl. Geol. Congress 97, 185–194 (1968).

Nichols, E. Geothermal Exploration Under the Salton Sea Using Marine Magnetotellurics. California Energy Commission, PIER Renewable Energy Technologies Program, CEC-500-2009-005, (2009).

O'Sullivan, J.P., Araya, N., Popineau, J., Renaud, T., Riffault, J.: An EWASG Natural State and Production Forecast Model of the Salton Sea Geothermal Field, Transactions GRC, 47 (2023a).

O'Sullivan, J., Popineau, J., Gravatt, M., Renaud, T., Riffault, J., Croucher, A., Yeh, A. & O'Sullivan M. "An integrated, mesh-independent geothermal modeling framework." Environmental Modeling and Software, 163, (2023b), 105666.

O'Sullivan J.P., Araya, N., Popineau, J., Renaud, T., Riffault, J., O'Sullivan M.: Investigating Reinjection Strategies to Optimise Lithium Production from the Salton Sea Geothermal Field, Proceedings, 49th Workshop on Geothermal Reservoir Engineering, Stanford University, Stanford, CA (2024) California, February 12-14, (2024)

Schmitt, A.K., Hulen J.B.: Buried rhyolites within the active, high-temperature Salton Sea geothermal system. Journal of Volcanology and Geothermal Research. 178 (2008) 708–718. https://doi.org/10.1016/j.jvolgeores.2008.09.001

Williams, A.E.: Fluid density distribution in a high temperature, stratified thermohaline system: implications for saline hydrothermal circulation. Earth and Planetary Science Letters 146 (1997) 121-136.

Williams, A.E., McKibben, M.A.: A Brine interface in the Salton Sea Geothermal System, California: Fluid geochemical and isotopic characteristics. Geochimica et Cosmochimica, 53, (1989), 1905-1920.